Biomechanical modelling of anther dehiscence and pollen release

Problem presented by

Z.A. Wilson, Centre for Plant Integrative Biology
zoe.wilson@nottingham.ac.uk

at the 4th Mathematics in the Plant Sciences Study Group,
Nottingham, 4–7 January, 2011

Contributors

M.R. Nelson, martin.nelson@nottingham.ac.uk
L.R. Band, leah.band@cpib.ac.uk
R.J. Dyson, r.j.dyson@bham.ac.uk
K.J. Heymer, pmxkjh@nottingham.ac.uk
J. Hiorns, pmxjh1@nottingham.ac.uk
O.E. Jensen, oliver.jensen@nottingham.ac.uk
A. Korn, pmxak@nottingham.ac.uk
T. Lessinnes, lessinnes@maths.ox.ac.uk
S. Pearce, simon.pearce@nottingham.ac.uk
S. Thomas, sophy.thomas@chester.ac.uk
D.L.K. Toner, d.l.k.toner@sms.ed.ac.uk
F. Xu, pmxfx@nottingham.ac.uk
C. Yang, cai-yun.yang@nottingham.ac.uk

Report compiled by

M.R. Nelson, martin.nelson@nottingham.ac.uk

March 16, 2011

Abstract

Understanding the processes which underlie pollen release is key to efficient production of hybrid crops. Pollen is produced in compartments termed *locules*, which reside within the anther. Surrounding the locules are two cell layers: an outer *epidermis* and an inner *endothecium*. During pollen development, endothecial cells undergo secondary thickening – a process by which cell walls are lined by a helical arrangement of lignin fibres, strengthening the layer and providing a natural resistance to bending. Pollen release occurs as a result of an anther dehiscence process, during which the anther wall splits, exposing the pollen to the environment. A number of processes have been proposed to drive this process. In this report, we examine one such process: that in which anther dehiscence is driven by dehydration of the epidermis, which results in contraction of this layer and an associated change to the preferred curvature of the locule. We extend an existing bilayer model to incorporate expansion and contraction of both cell layers, and use cell-scale models to determine the associated parameters in terms of experimentally measurable quantities. We present brief experimental validation of this hypothesis, in which the response of lily anthers to external hydration/dehydration is observed, and use the associated biomechanical model to explain the observed changes in the anther's configuration.

1 Introduction

Plant reproduction and the formation of viable gametes (reproductive cells) is critical to fertilisation and seed formation, and is thus essential to the production of most of the food that we eat. It plays a critical role in breeding systems and in the production of hybrid crops which, although difficult and costly to generate, frequently out-yield inbred lines by 20–30%. The combination of population growth, climate change and the reduction of available agricultural land mean that it is essential that we develop sustainable, effective agricultural systems that give increased yield but are less damaging to the environment. Achieving these goals requires a deeper understanding of plant reproduction, particularly the formation and release of pollen, that will enable the development of strategies to aid hybrid development and thus food security.

Pollen is formed within specialised organs, stamen, in the flower (figure 1). These are comprised of a wider upper region that forms the anther, containing the pollen, and a stalked region, the filament, containing the vascular bundles (transport system in higher plants), which extends to maximise dispersion of the pollen. The timing of pollen release is highly controlled to maximise the chances of fertilisation and is regulated partly by the developing pollen grains and partly by the developing maternal anther. Figure 1 illustrates a cross-section of the anther. Prior to opening, pollen is contained within four compartments termed *locules*. Locules are situated in pairs; the region between the two locules is termed the *septum*, the most external point of which is termed the *stomium*. Anther dehiscence (opening of the anther to allow pollen release) is associated with a number of biomechanical changes within the septum and stomium. The anther comprises four maternal cell layers: the outer epidermis, the endothecium, the middle cell layer, and the tapetum. Within the locule are the inner sporogenous cells which will form the pollen.

Anther dehiscence involves a series of steps, including differentiation of the cellular layers in the anther, formation of secondary thickening of cell walls within the endothecium, enzymatic digestion of septum and stomium cell walls, differential expansion, dehydration and pollen swelling (Bonner & Dickinson, 1989; Keijzer, 1987; Scott *et al.*, 2004). These processes cause the cells of the septum and stomium to be weakened and generate various mechanical tensions within the anther, resulting in breakage and opening. Many mutants have been identified which fail to release their pollen (dehiscence mutants) due to defects in these various stages. Preliminary biological models have been developed to explain the processes and forces involved in anther opening; however, no mathematical modelling of this process has been carried out and we currently do not know what are the critical aspects and physical features of this important

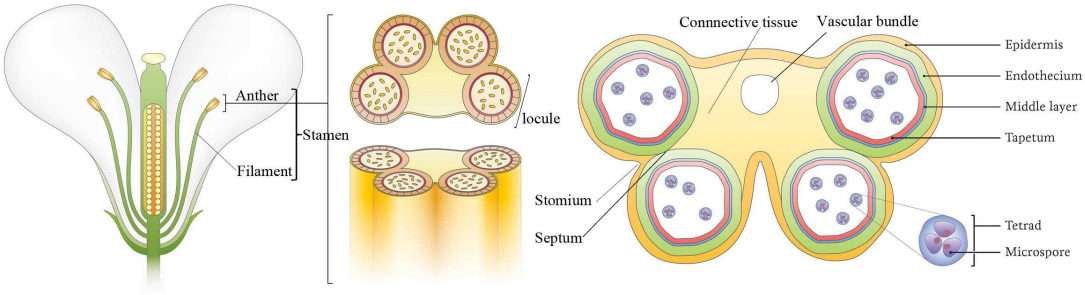

Figure 1: Left: Structure of the flower and anther. Right: Diagram of a cross-section through the anther, showing the four cell layers of the anther – the outer epidermis, the endothecium, the middle cell layer and the tapetum. Inside each locule reside microspores (visible at this stage as tetrads), that will eventually form the mature pollen. Figure taken from Wilson *et al.* (2011).

developmental stage.

1.1 Degeneration and breakage of the septum and stomium

Anther dehiscence is thought to involve cell-wall-degrading enzymes which break down the pectin in the cell walls. Several hydrolytic enzymes and proteins linked to cell wall loosening are thought to be involved, including polygalacturonases (PGs), -1,4- glucanases, and expansins. These enzymes are likely to be regulated by plant hormones (including jasmonic acid (JA), ethylene and abscisic acid (ABA)).

Initially degeneration of the septum occurs, generating a bilocular anther, which is followed by stomium cell breakage and then retraction of the anther and pollen release (figure 2). The importance of a functional stomium for dehiscence has been demonstrated by failure of tobacco dehiscence after specific cell ablation of the stomium. Prior to dehiscence the stomium undergoes cell death and splitting, this does not appear to require viable pollen to be present since splitting is still seen in male sterile lines without viable pollen. This breakage appears to be due to weakening of the septum and stomium due to enzymatic digestion, combined with expansion of the pollen and anther wall.

The anther septum and stomium breakdown is also thought to be via a process related to programmed cell death (PCD). There have been a number of reports of dehiscence mutants resulting from changes to endothecium and stomium degeneration, which result in endothecium degeneration and indirectly inhibit breakage of the stomium, although the pollen appears normal.

1.2 Endothecial secondary thickening

After meiosis and formation of the immature pollen, the endothecium undergoes selective deposition of secondary thickening whilst the stomium and septum do not. This localised thickening is critical for subsequent anther opening. Endothecium development is coordinated with pollen maturation and the degeneration of the anther tapetum and middle layer.

The process of pollen development in *Arabidopsis thaliana* has been separated into 15 stages based on anther development. In the Arabidopsis anther, the endothecium is first established during anther stage 5. It undergoes expansion during anther stages 6–10 and develops secondary cell wall thickening during anther stage 11, at which point bar-like ligno-cellulose fibrous bands are deposited. Endothecium secondary thickening appears to be essential for providing the mechanical force for anther dehiscence. This has been demonstrated experimentally with Arabidopsis male sterile mutants, for example myb26 (Dawson *et al.*, 1999) and the NAC secondary wall thickening promoting factor1 (nst1)nst2 double mutant (Mitsuda et al., 2007). In the myb26 mutant, anther development appears normal up to anther stage 11; however, during the later stages, the lingo-cellulosic wall thickenings seen in the wild type anther endothecium wall, do not form. Degradation of the septum and formation of stomium take place normally; however, the endothecial cells fail to expand, then collapse and the subsequent shrinkage of the anther walls does not occur, resulting in failure of pollen release (Dawson *et al.*, 1999).

1.3 Opening the anther

Observations of dehiscence in *Gasteria verrucosa* suggest that as pollen wall formation occurs, the epidermal and endothecial cells lose some of their starch, which may affect the osmotic potential within the cell, leading to water flow and changes in hydrostatic pressure. These cells then start tangential and radial expansion, which is followed by endothecial secondary thickening (Keijzer, 1987). However, the stomium and septum do not undergo secondary thickening. The septum undergoes enzymatic lysis, reducing the adhesion between neighbouring cells, alongside the mechanical swelling of the bordering epidermal cells, facilitating stomium opening (Keijzer, 1987). Tangential swelling of the epidermis and endothecium increases the circumference of the locule wall; however, because the endothecium walls have secondary thickening, the inner locule wall dimensions are fixed. The combination of outer enlargement and inner fixed dimensions causes the locule wall to bend inwards causing disruptions to the

stomium cells (figure 2). The stomium cells are then mechanically broken by inward bending of the adjacent locule walls. The swelling of the pollen grains has also been proposed as a factor in generating the force required for final locule rupture in rice (figure 2).

1.4 Dehydration of the anther wall

The final stages of anther dehiscence involve the dehydration of the endothecium and epidermal cells, which cause the locule to bend outwards (figure 2). It has been suggested that this occurs, at least in part, as a consequence of evaporation but is more likely due to active removal of water from the anther. Observations of the water status of tomato anthers revealed differential regions of anther dehydration. Conversion of starch to sugar may create variations in the osmotic potential within the anther tissues, providing a mechanism for selective dehydration (regions of low osmotic potential dehydrate more readily). This has been supported by data on localised sucrose transport around the anther tissues (Stadler *et al.*, 1999).

It has also been suggested that movement of potassium ions from the anther locule, prior to dehiscence, into the pollen grains may play a role in attracting water from the surrounding regions, causing the swelling of the endothecium and pollen prior to anther opening. This swelling of the pollen may be partly responsible for stomium rupture. Water translocation frequently occurs via plasmodesmata connections between adjacent cells; however, a large gene family encoding aquaporin proteins have been shown to mediate the passive movement of water between cells. Some aquaporins have been identified specifically within the anther: these will influence cell wall permeability and water movement in the anther. It therefore seems likely that an active process of selected dehydration is occurring within the anther that acts to provide the final force for anther opening (figure 2).

1.5 The aims of this study

In this study we develop a mathematical model that focuses upon the role of epidermal and endothecial dehydration in driving anther dehiscence, neglecting the effects of changes in locule pressure. To validate this proposed mechanism, proof of principle experiments were carried out in which Lily anthers were hydrated under a microscope, and changes in shape were recorded. Two stages of Lily anthers that had already split at the septum and stomium were used: i) those which were already fully open, and ii) those which were close to opening but not yet fully open. Younger anthers that had not

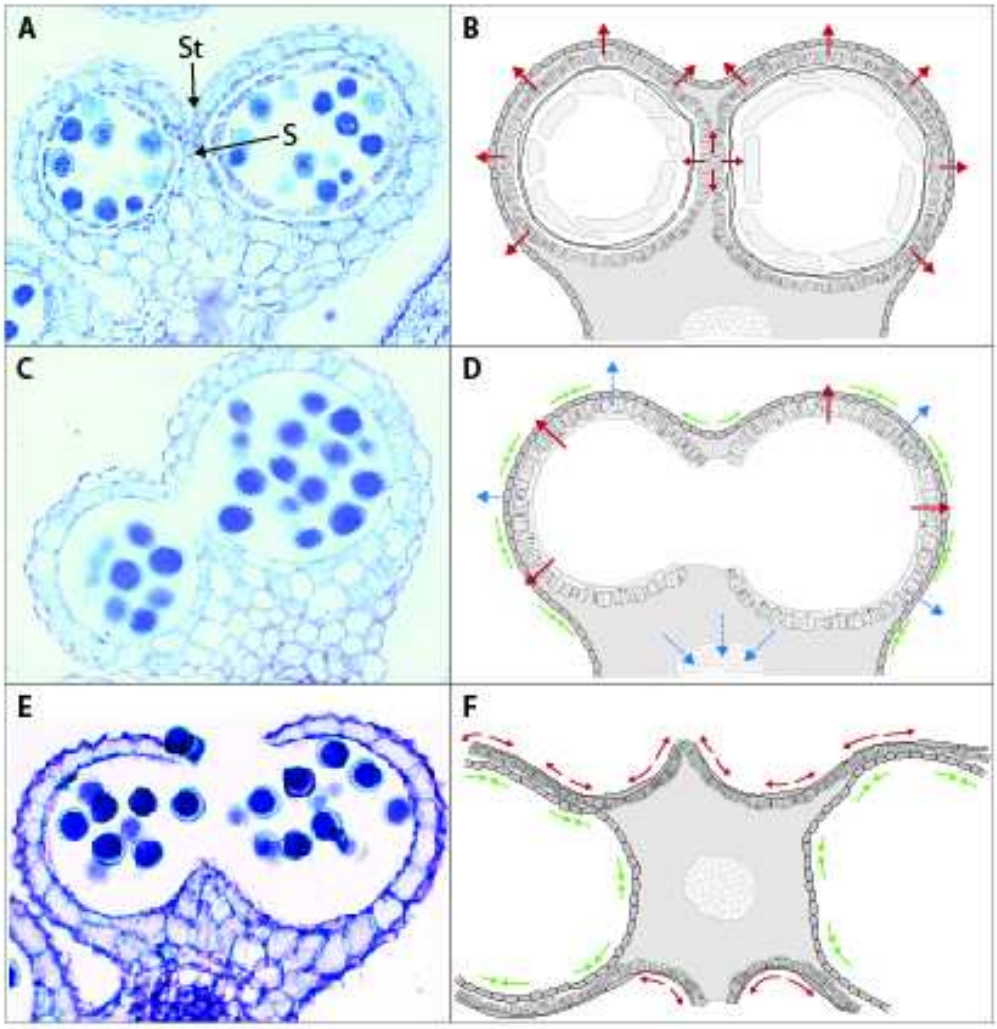

Figure 2: Image taken from Wilson *et al.* (2011), showing previously postulated biomechanical mechanisms which may contribute to anther dehiscence. (A) Microspore release, the tapetum starts to breakdown and the endothecium expands and secondary thickening is deposited. As the pollen expands there is a postulated outward pressure (B, red arrows) exerted from the inside of the locule on the anther, which increases in size. However, the bands of secondary thickening in the endothecium restrict expansion causing increased tension (D, green arrows). (B) Enzymatic lysis of the stomium combined with the pressure from the expansion of the pollen causes the septum to break to form a single locule (C,D). At this point the anther walls begin to dehydrate due to evaporation and active water transport (D, blue arrows) causing the shrinkage of the epidermal cells, resulting in an increased tension on the stomium.

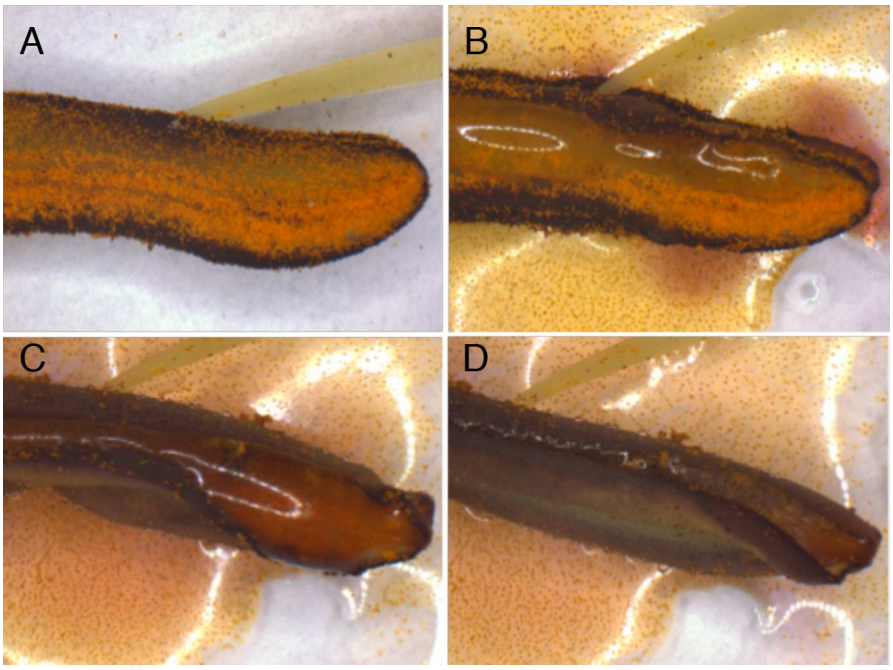

Figure 3: Lily anther closing based on hydration status. (A) Fully opened anther. (B) Anther with water droplet, showing start of closing. (C) Approximately 15 mins after water treatment anther is actively closing. (D) Approximately 30 mins after water treatment anther is almost fully closed.

split at the stomium did not appear to be under pressure, since when cut they did not burst open and release their locule contents.

Anthers that were fully open had a small amount of water placed onto their surface (figure 3), these anthers then rapidly started to re-close and over a period of approximately 30 mins closed completely (figure 3D). However, if sections were cut through the anther and then placed in the water droplets the resultant movement and closure of the anther was extremely rapid (5–10 secs). This increased speed may have been due to greater hydration of the epidermal and anther wall tissues, since the anther is an extremely hydrophobic surface.

Anthers that were near to opening but were not fully open, when left on a microscope slide in the light, progressively opened as they dehydrated.

These preliminary results justify our model assumption, that hydration is a key mechanism in driving anther dehiscence. While locule pressure does not seem sufficient to drive dehiscence independently, we still incorporate a locule pressure in our model for completeness. Our model demonstrates the importance of secondary thickening in endothecial cells in enabling contractile forces arising from dehydration to be converted into bending forces that promote anther opening.

Figure 4: Lily anther that was closed, which started to open as it dehydrated on the slide under the microscope light.

2 The model

We formulate a two-dimensional model for a cross-section of the anther under the assumption of plane strain. We assume that anther dehiscence is primarily driven by dehydration of the epidermis and endothecium, which causes contraction of the cells in these layers. Focusing upon the situation in which the two cell layers are fully adhered, we consider a mechanism by which differences in the rates of expansion/contraction of these layers may induce a change in the preferred curvature of the composite structure, stimulating bending which ultimately enables the anther to open. We adapt the bilayer model of Nelson *et al.* (2011) to describe these changes in preferred curvature as a function of the turgor pressure of the epidermal cell layer. Since the cells of the endothecium are surrounded by lignin fibres arranged into a tight helix, we assume that this layer has a natural resistance to bending. By comparison, we assume that the bending resistance of the epidermis is negligible; dehydration of the epidermis generates an in-plane tension F_T^{+*} therein, transmitting a force to the endothecium which induces bending. Throughout the forthcoming discussion, stars distinguish dimensional quantities from their dimensionless counterparts. Terms with '$+$' superscripts refer to the epidermis, while those with '$-$' superscripts refer to the endothecium.

We examine configurations belonging to three distinct cases. Firstly, we consider an intact septum which provides a restoring force F_{sep}^*, holding the stomium in place. Keeping all hydration parameters fixed, we initially examine solutions for decreasing F_{sep}^* to model degradation of the septum. We identify the state in which $F_{sep}^* = 0$ with the septum breaking. In our second case, the septum is absent and we drive geometric changes through changes to the preferred length of the epidermis, resulting from dehydration thereof. The third case is that which follows breaking of the stomium, allowing the anther to open. In this case, we allow the epidermis to further dehydrate,

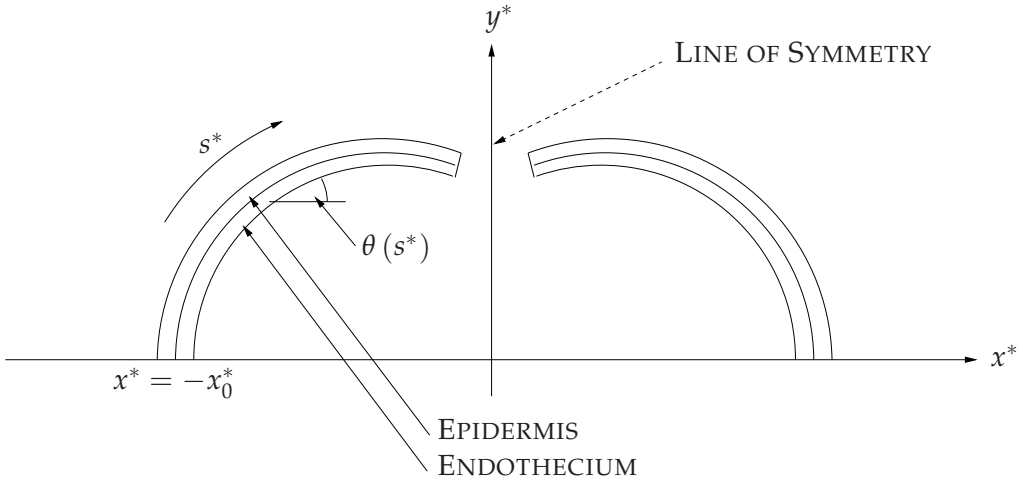

Figure 5: Geometry of the anther segment under consideration, and associated coordinate systems. The composite layer comprises epidermal and endothecial cell layers, which we assume to always remain tangential and adjacent to one another.

gradually changing the resulting preferred configuration from concave to convex. We describe these three cases, and the corresponding boundary conditions, more fully in section 2.1. We begin, however, with a discussion of the equations which govern the biomechanics of the anther segment.

Assuming symmetry about the septum, we restrict attention to one locule. Furthermore, as a first approximation, we assume the lower half of this locule to be rigid and present solely a model for the upper half. We denote by L_0^* the undeformed arclength of the bilayer. The angle of inclination of the composite to the horizontal is denoted by $\theta(s^*)$, where s^* is a measure of arclength. We also describe the geometric configuration of the bilayer in terms of Cartesian coordinates x^* and y^*, respectively oriented horizontally and vertically and related to $\theta(s^*)$ via:

$$\frac{\mathrm{d}\,x^*}{\mathrm{d}\,s^*} = \cos\theta, \qquad \frac{\mathrm{d}\,y^*}{\mathrm{d}\,s^*} = \sin\theta. \tag{1}$$

The curvature of the bilayer, κ^*, is given by

$$\kappa^* = \frac{\mathrm{d}\,\theta}{\mathrm{d}\,s^*} \tag{2}$$

We denote tangential and normal stress resultants (per unit length) in the endothecium by F_T^{-*} and F_N^{-*} respectively; variations in these stress resultants generate a bending moment (per unit length) M^*. Between the endothecium and the epidermis act a frictional stress Q^* and normal reaction R^*, as shown in figure 6. We also incorporate a locule pressure p^*, measured relative to atmospheric pressure, which acts to deform the composite structure from below.

We denote tangential and normal unit vectors by $\hat{\mathbf{t}}$ and $\hat{\mathbf{n}}$, which are defined according to:

$$\hat{\mathbf{t}} = (\cos\theta, \sin\theta), \qquad \hat{\mathbf{n}} = (\sin\theta, -\cos\theta), \tag{3}$$

and related via

$$\frac{\mathrm{d}\,\hat{\mathbf{t}}}{\mathrm{d}\,s^*} = -\kappa^*\hat{\mathbf{n}}, \qquad \frac{\mathrm{d}\,\hat{\mathbf{n}}}{\mathrm{d}\,s^*} = \kappa^*\hat{\mathbf{t}}. \tag{4}$$

Balancing forces upon an arbitrary endothecial element of length $\mathrm{d}\,s^*$ (as shown in figure 6), we have

$$\left(F_T^{-*}\hat{\mathbf{t}}\right)\Big|_{s^*+\mathrm{d}\,s^*} - \left(F_T^{-*}\hat{\mathbf{t}}\right)\Big|_{s^*} + \left(F_N^{-*}\hat{\mathbf{n}}\right)\Big|_{s^*+\mathrm{d}\,s^*} - \left(F_N^{-*}\hat{\mathbf{n}}\right)\Big|_{s^*} - Q^*\,\mathrm{d}\,s^*\hat{\mathbf{t}} + (R^* - p^*)\,\mathrm{d}\,s^*\hat{\mathbf{n}} = 0. \tag{5}$$

Taylor expanding those terms evaluated at $s^* + \mathrm{d}\,s^*$, truncating terms of $O\left(\mathrm{d}\,s^{*2}\right)$ and noting (4), the tangential and normal components of (5) give

$$\frac{\mathrm{d}\,F_T^{-*}}{\mathrm{d}\,s^*} + F_N^{-*}\kappa^* - Q^* = 0, \qquad \frac{\mathrm{d}\,F_N^{-*}}{\mathrm{d}\,s^*} - F_T^{-*}\kappa^* + R^* - p^* = 0. \tag{6}$$

A balance of moments upon the same element, assuming that the contribution of F_T is $O\left(\mathrm{d}\,s^{*2}\right)$, gives

$$\frac{\mathrm{d}\,M^*}{\mathrm{d}\,s^*} - F_N^{-*} + Q^*h^* = 0, \tag{7}$$

to leading order, where $2h^*$ is the thickness of the endothecium. The Q^*h^* term in (7) was not included in the analysis of Nelson *et al.* (2011); we estimate its magnitude below.

Taking a discrete representation of the upper cell layer, and assuming θ is slowly varying between adjacent cells, Nelson *et al.* (2011) derived the following expressions for Q^* and R^*:

$$Q^* = -\frac{\mathrm{d}\,F_T^{+*}}{\mathrm{d}\,s^*}, \qquad R^* = -\kappa^*F_T^{+*}. \tag{8}$$

Introducing the composite in-plane tension $F^* = F_T^{-*} + F_T^{+*}$, (6–8) give

$$\frac{\mathrm{d}\,F^*}{\mathrm{d}\,s^*} = -\kappa^*F_N^{-*}, \qquad \frac{\mathrm{d}\,F_N^{-*}}{\mathrm{d}\,s^*} = \kappa^*F^* + p^*, \qquad \frac{\mathrm{d}\,M^*}{\mathrm{d}\,s^*} = F_N^{-*} + h^*\frac{\mathrm{d}\,F_T^{+*}}{\mathrm{d}\,s^*}. \tag{9}$$

We prescribe the following constitutive assumptions, governing the extensions of the cell layers:

$$F_T^{\pm*} = k^{-*}\left(\lambda^{\pm} - \lambda_0^{\pm}\right), \tag{10}$$

in which $\lambda^{\pm}$ are the in-plane stretches of the two layers, $\lambda_0^{\pm}$ are dimensionless variables which describe the resting lengths of the layers, and $k^{\pm*}$ are extensional stiffness parameters. In the endothecium, we consider these quantities to be evaluated on the

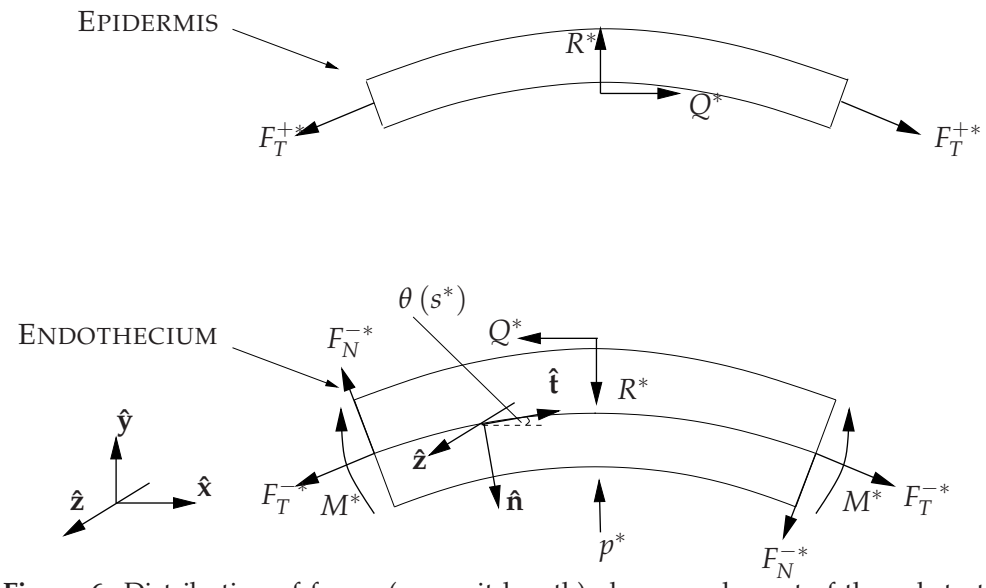

Figure 6: Distribution of forces (per unit length) along an element of the substrate, the resultant stresses and bending moments. Clockwise arrows indicate bending moments acting the negative $\hat{\mathbf{z}}$-direction.

centreline. Endothecial secondary thickening is incorporated into the model via an increase in k^{-*}. Assuming that the frictional force, Q^*, is sufficient for perfect adhesion, and taking $\kappa^* h^* \ll 1$, we set $\lambda \equiv \lambda^+ = \lambda^-$ so that the net in-plane tension is given by

$$F^* = \left(k^{+*} + k^{-*}\right)\lambda - \left(k^{+*}\lambda_0^+ + k^{-*}\lambda_0^-\right). \tag{11}$$

In (11), the first term represents the composite extensibility while the second is influenced by hydration of both cell layers.

We now require a constitutive assumption relating bending moments to curvatures. We assume

$$M^* = D^*\left(\kappa^* - \tilde{\kappa}_0^*\right), \tag{12}$$

where D^* is the endothecial resistance to bending and $\tilde{\kappa}_0^*$ represents the preferred curvature of the endothecium in the absence of the epidermis; we assume $\tilde{\kappa}_0^*$ is spatially uniform.

Substitution of (10) and (12) into (9c) gives

$$\frac{\mathrm{d}\,\kappa^*}{\mathrm{d}\,s^*} = \frac{F_N^{-*}}{D^*} + \frac{\mathrm{d}\,\kappa_0^*}{\mathrm{d}\,s^*}, \tag{13}$$

where $\kappa_0^* = \tilde{\kappa}_0^* + h^* k^{+*}\left(\lambda - \lambda_0^+\right)/D^*$ can be interpreted as an effective preferred curvature of the composite layer, incorporating the contraction/expansion of the epidermis. We can represent epidermal dehydration by a reduction in λ_0^+, causing κ_0^* to increase.

It is convenient to rewrite the governing equations in terms of the Lagrangian arc-length variable $\tilde{s}^*$, related to s^* via:

$$\frac{\mathrm{d}\, s^*}{\mathrm{d}\,\tilde{s}^*} = \lambda. \tag{14}$$

We nondimensionalise the problem by scaling lengths against the resting length of the composite (L_0^*), curvatures against $1/L_0^*$, stress resultants against k^{-*} and locule pressure against k^{-*}/L_0^*. Denoting $N = F_N^{-*}/k^{-*}$, equations (9a,b), (13), (1) and (2) then become

$$\frac{\mathrm{d}\, F}{\mathrm{d}\,\tilde{s}} = -\lambda\kappa N, \qquad \frac{\mathrm{d}\, N}{\mathrm{d}\,\tilde{s}} = \lambda\kappa F + \lambda p, \qquad \frac{\mathrm{d}\,\kappa}{\mathrm{d}\,\tilde{s}} = \alpha\lambda N + \Phi\frac{\mathrm{d}}{\mathrm{d}\,\tilde{s}}\left(\lambda - \lambda_0^+\right), \tag{15a}$$

$$\frac{\mathrm{d}\,\theta}{\mathrm{d}\,\tilde{s}} = \lambda\kappa, \qquad \frac{\mathrm{d}\, x}{\mathrm{d}\,\tilde{s}} = \lambda\cos\theta, \qquad \frac{\mathrm{d}\, y}{\mathrm{d}\,\tilde{s}} = \lambda\sin\theta, \tag{15b}$$

with F given by

$$F = (1+\beta)\,\lambda - \left(\lambda_0^- + \beta\lambda_0^+\right). \tag{16}$$

The above system is dependent upon three dimensionless parameters: $\alpha = k^{-*}L_0^{*2}/D^*$, which captures the endothecial resistance to extension relative to its resistance to bending; $\beta = k^{+*}/k^{-*}$, which captures the stiffness of the epidermis relative to that of the endothecium; and $\Phi = \alpha\beta h^*/L_0^*$, which captures the extent to which hydration of the epidermis generates changes in the preferred curvature of the endothecium.

2.1 Boundary conditions

We solve (15–16) subject to boundary conditions which describe three distinct cases (see figure 7). In all of these cases, we clamp the bilayer at $\tilde{s} = 0$ as follows:

$$\theta = \frac{\pi}{2}, \qquad x = -x_0, \qquad y = 0 \qquad \text{on } \tilde{s} = 0, \tag{17}$$

where $x_0 = x_0^*/L_0^*$ is the locule width scaled against the natural length of the anther segment.

The first stage of the anther dehiscence process is that in which the septum is intact, providing a restoring force F_{sep} to keep the stomium in place. In this so-called "case I", we set:

$$\text{Case I:} \quad x = 0, \quad F_{sep} = 2F\sin\theta - 2N\cos\theta, \qquad \kappa = \tilde{\kappa}_0 + \Phi\left(\lambda - \lambda_0^+\right) \qquad \text{on } \tilde{s} = 1, \tag{18}$$

in which the final boundary condition forces the bending moment at the symmetry boundary to vanish. We assume that as the septum degrades, F_{sep} gradually decreases from some initial positive value, until $F_{sep} = 0$ when the septum 'breaks'. Throughout

case I, we keep all mechanical properties fixed. In particular we neglect dehydration in case I, fixing λ_0^+.

We label the intermediate case in which the septum has broken but the stomium remains intact as "case II". Throughout case II, we have $F_{sep} = 0$ and we require

$$\text{Case II:} \quad x = 0, \quad 2F\sin\theta - 2N\cos\theta = 0, \qquad \kappa = \tilde{\kappa}_0 + \Phi\left(\lambda - \lambda_0^+\right) \qquad \text{on } \tilde{s} = 1. \tag{19}$$

Changes to the anther's configuration are now driven by dehydration of the epidermis; we gradually decrease λ_0^+ from its initial positive value (which may be determined experimentally as a function of the turgor pressure, see section 2.2.1). As λ_0^+ decreases, and the preferred curvature evolves, we monitor the horizontal force exerted upon the symmetry boundary, given by

$$F_{contact} = 2F\cos\theta + 2N\sin\theta. \tag{20}$$

Once this force decays to zero, we enter "case III" in which the boundary at $\tilde{s} = 1$ moves away from the symmetry line, mimicking the opening of the anther. We continue to reduce λ_0^+ and the anther continues to open. Thus, the locule pressure is released and we set $p = 0$. In case III, all forces upon the boundary vanish and the preferred curvature is attained. Thus, we impose

$$\text{Case III:} \qquad F = 0, \qquad N = 0, \qquad \kappa = \tilde{\kappa}_0 + \Phi\left(\lambda - \lambda_0^+\right) \qquad \text{on } \tilde{s} = 1. \tag{21}$$

2.2 Parameter estimation

In table 1, we summarise the dimensional parameters in the model. It should be possible to source estimates for L_0^*, x_0^*, p^*, $\tilde{\kappa}_0^*$ and h^* from the literature. In the following simulations, we shall assume, for simplicity, that the endothecium is naturally flat and set $\tilde{\kappa}_0^* = 0$. We use the model to the investigate the influence of the locule pressure on the dynamics. In addition, we set $x_0^* = 2L_0^*/\pi$ for convenience.

We estimate the remaining parameters via a cell-scale model of the endothecium.

2.2.1 Cell-scale model of the epidermis

We can determine the epidermal parameters, k^{+*} and λ_0^+, in terms of cell-scale parameters by balancing forces in an arbitrary epidermal cell. Treating each epidermal cell as a rectangular box of height H^*, with elastic walls extending due to turgor pressure (per unit length) p^{+*}, the in-plane stress resultant (per unit length) is given by

$$F_T^{+*} = 2E^{+*}\left(\lambda^+ - 1\right) - p^{+*}H^*. \tag{22}$$

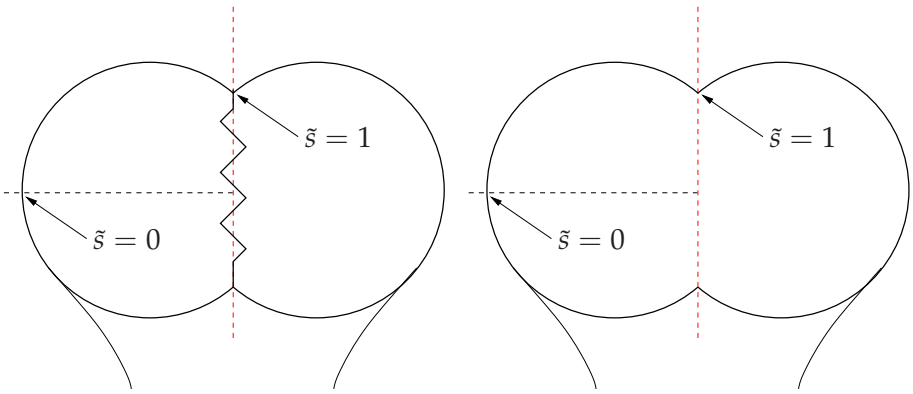

(a) Case I: Septum intact

(b) Case II: After septum breaks

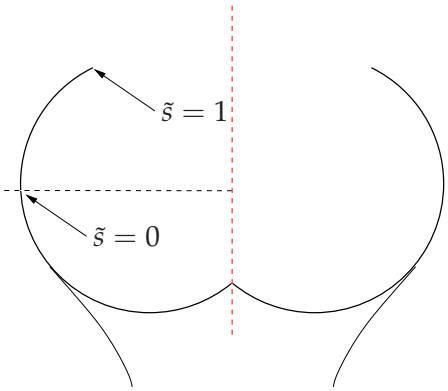

(c) Case III: Anther opens

Figure 7: The three cases considered here. Red dotted lines illustrate the line of symmetry at the septum. Black dotted lines demark the upper half of the locule, which we model here.

for epidermal Young's modulus E^{+*}. Comparing (22) with (10), we have $k^{+*} = 2E^{+*}$ and

$$\lambda_0^+ = 1 + p^{+*}\left(H^*/k^{+*}\right) \equiv 1 + P^+. \tag{23}$$

We, therefore, consider solutions for a reference state with $\lambda_0^+ > 1$ and allow epidermal dehydration to reduce the turgor pressure P^+, so that λ_0^+ gradually tends to unity.

2.2.2 Cell-scale model of the endothecium

In contrast to the epidermis, the endothecial cell walls have secondary thickening which comprises stiff lignin fibres which form a helical spring around the cell. These fibres cause the endothecium to resist bending. We assuming that the lignin fibres provide the dominant mechanical contribution to the endothecial cells, and that the remainder of the cell wall does not contribute to the bending or extensional stiffnesses. Denoting

Parameter	Description	Value
L_0^*	Natural length of the segment of bilayer	
x_0^*	Width of the locule	$2L_0^*/\pi$
p^*	Locule pressure	
$\tilde{\kappa}_0^*$	Natural curvature of the endothecium	≈ 0
h^*	Half the endothecium thickness	$2.5\,\mu$m
D^*	Bending stiffness of endothecium	see (26)
k^{+*}	Extensional stiffness of epidermis	see §2.2.1
k^{-*}	Extensional stiffness of endothecium	see §2.2.2
λ_0^+	Natural length of epidermis	see §2.2.1
λ_0^-	Natural length of endothecium	see §2.2.2

Table 1: Parameter values in the tissue-scale model.

the extensional stiffness of the helical spring by k_f^*, and regarding a typical endothecial cell as an extensible rectangular box as in 2.2.1, a force balance upon a typical cell suggests that

$$F_T^* = 2k_f^*(\lambda - 1) - 2h^* p^{-*}, \tag{24}$$

where p^{-*} is the turgor pressure of the endothecial cell, and E^{-*} is the stiffness of the endothecial cell wall in the absence of the lignin fibres. Comparing (24) with (10), we see that macro-scale parameters may be given in terms of cell-scale quantities as follows:

$$k^{-*} = 2k_f^*, \quad \lambda_0^- = \frac{k_f^* + h^* p^*}{k_f^*}. \tag{25}$$

The cell-scale parameters which determine D^*, k^{-*} and λ_0^- are summarised in table 2. Again, appropriate estimates of parameters would need to be sourced from the literature or future experiments. However, we can deploy the results of previous studies of helices to estimate the relative sizes of these parameters. We denote the Young's modulus of the lignin fibres by E_f^*, their Poisson ratio by ν_f, and their radius by R_f^*. The calculation of Costello (1977) then gives the bending stiffness of the helical spring as

$$D_{cell}^* = \frac{E_f^* \pi R_f^{*4} \sin\gamma}{2(2 + \nu_f \cos^2\gamma)}, \tag{26}$$

where γ is the pitch angle. The endothecial cells are approximately $10 - 20\,\mu$m long with approximately 5 turns of the helix per cell; we calculate the pitch angle to be in the region of $\gamma = 7 - 14^\circ$. In addition, let us denote the extensional stiffness of the

Parameter	Description	Value
p^{+*}	Turgor pressure of epidermal cells	
H^*	Height of epidermal cells	
E^{+*}	Stiffness of epidermal cell walls	
R_f^*	Radius of lignin fibres	25 nm
k_f^*	Stiffness of lignin fibres	see (27)
E_f^*	Young's modulus of lignin fibres	
ν	Poisson ratio of lignin fibres	≈ 1
γ	Pitch angle of lignin helical spring	$7 - 14^\circ$

Table 2: Parameter values in the cell-scale models of the epidermis and endothecium.

helical spring by k_{cell}^*. From Love (1944), we have

$$k_{cell}^* = \frac{E_f^* \pi R_f^{*4} \sin\gamma}{4h^{*2}} \left(\frac{\cos^2\gamma}{1+\nu_f} + \sin^2\gamma \right). \tag{27}$$

The quantities D_{cell}^* and k_{cell}^* represent the bending stiffness and extensional stiffness of a single endothecial cell. We expect these values to contribute to the expressions for similar macroscopic quantities for sheets of endothecial cells. From (26) and (27), we expect that

$$\frac{k^{-*}h^*}{D^*} \sim \frac{k_{cell}^* h^*}{D_{cell}^*} \sim 1. \tag{28}$$

The above suggests that endothecial secondary thickening results in a high resistance to stretching and a low resistance to bending, potentially allowing shrinkage of the epidermis to bend the composite structure.

2.2.3 Dimensionless parameter groupings

After nondimensionalisation, the model depends on the dimensionless parameter groupings summarised in table 3. We expect the epidermal resistance to extension to be less than that of the endothecium, $\beta \ll 1$ and the endothecial resistance to extension to be much greater than its resistance to bending, $\alpha \gg 1$. The formula for the parameter grouping Φ can be rearranged to give

$$\Phi = \beta \frac{k^{-*} L_0^* h^*}{D^*} \sim \beta \frac{L_0^*}{h^*}, \tag{29}$$

in which the latter expression follows from (28). Since $\beta \ll 1$ and $h^* \ll L_0^*$, we conclude that it is appropriate to let $\Phi = O(1)$.

Parameter	Description	Formula
x_0	Ratio of locule width to natural length of anther segment	x_0^*/L_0^*
α	Ratio between endothecial resistance to extension and resistance to bending	$k^{-*}L_0^{*2}/D^*$
β	Ratio of epidermal to endothecial resistance to extension	k^{+*}/k^{-*}
Φ	Ratio of resistance of epidermal extension to endothecial bending	$\alpha\beta h^*/L_0^*$

Table 3: The dimensionless parameter groupings that govern the model dynamics.

2.3 The limit $\alpha \gg 1$

Suppose $\alpha \gg 1$, $\Phi = O(1)$ and β is at most $O(1)$. We can then rescale dependent variables according to

$$N = \hat{N}/\alpha, \qquad F = \hat{F}/\alpha, \qquad p = \hat{p}/\alpha, \tag{30}$$

reducing (15a) to

$$\frac{\mathrm{d}\,\hat{F}}{\mathrm{d}\,\tilde{s}} = -\lambda\kappa\hat{N}, \qquad \frac{\mathrm{d}\,\hat{N}}{\mathrm{d}\,\tilde{s}} = \lambda\kappa\hat{F} + \lambda\hat{p}, \qquad \frac{\mathrm{d}\,\kappa}{\mathrm{d}\,\tilde{s}} = \lambda\hat{N} + \Phi\frac{\mathrm{d}}{\mathrm{d}\,\tilde{s}}\left(\lambda - \lambda_0^+\right), \tag{31}$$

with $\hat{F}$ given by

$$\frac{\hat{F}}{\alpha} = (1+\beta)\,\lambda - \left(\lambda_0^- + \beta\lambda_0^+\right). \tag{32}$$

To leading order in α^{-1}, we have

$$\lambda = \frac{\lambda_0^- + \beta\lambda_0^+}{1+\beta}. \tag{33}$$

It follows that

$$\lambda - \lambda_0^+ = \frac{\lambda_0^- + \beta\lambda_0^+ - (1+\beta)\,\lambda_0^+}{1+\beta} = \frac{\lambda_0^- - \lambda_0^+}{1+\beta}. \tag{34}$$

Thus, provided that λ_0^+ and λ_0^- are spatially uniform, (31) implies that (in terms of Eulerian coordinates)

$$\kappa\frac{\mathrm{d}\,\kappa}{\mathrm{d}\,s} = -\frac{\mathrm{d}\,\hat{F}}{\mathrm{d}\,s} \Longrightarrow \frac{1}{2}\kappa^2 + \hat{F} = C, \tag{35}$$

for some constant C. Thus, (31) implies that

$$\frac{\mathrm{d}^2\,\kappa}{\mathrm{d}\,s^2} = \kappa\left(C - \frac{1}{2}\kappa^2\right) + p, \tag{36}$$

and the problem reduces to that of a classical Euler–Bernoulli beam. Configurations are determined entirely by the length of the composite structure, appearing in the boundary conditions which are now applied at $s = 0$ and $s = (\lambda_0^- + \beta\lambda_0^+)/(1+\beta)$.

3 Results

Here, we examine solutions to (15–21) determined using the MATLAB boundary value solver `bvp4c`. Figure 8 illustrates the sequence of configurations attained in cases I–III, for $\alpha = 1000$, $\beta = 0.01$, $\Phi = 1$, $\lambda_0^- = 1$, $\tilde{\kappa}_0 = 0$, $x_0 = 2/\pi$ and $p = 0$, while figure 9 illustrates corresponding stresses and strains. In panel (a), case I solutions are illustrated for $\lambda_0^+ = 3.5$ and F_{sep} decreasing in uniform steps of size 0.0001 from an initial value of 0.0011, representing degradation of the septum independently of dehydration in the epidermis. As F_{sep} decreases to zero (as indicated by the arrow), the configuration slowly lifts until $F_{sep} = 0$, when we make the transition to case II. In case II (panel (b)), dehydration of the epidermis generates changes in the preferred configuration, with λ_0^+ decreasing from 3.5 (as shown by the arrows). As λ_0^+ decreases, we monitor the contact force given by (20). For $\lambda_0^+ = 2.5$, the contact force vanishes and we enter case III, in which the anther opens (panel (c)). Configurations are now simply arcs of circles; the composite is stress free as illustrated by figure 9(g,h).

Simulations for small but non-zero locule pressure p show that the geometry of configurations is little changed from those of figure 8. Figure 10 illustrates case II and case III solutions for $p = 0.01$. In case II, since there are now two mechanisms driving the dehiscence process (epidermal dehydration and locule pressure), the anther can open for larger λ_0^+. However, as soon as the anther opens a little, the locule pressure is released ($p = 0$) and the anther would briefly close once more, into a configuration which is not well-described by our current model. Continued dehydration of the epidermis ultimately results in the anther opening once more, for $\lambda_0^+ \simeq 2.5$ for the parameter choice of figure 8.

4 Discussion

A key conclusion of our model is that the turgor pressure of the epidermal cells affects the resting length of the epidermis, which in turn affects the preferred curvature of the composite bilayer. We predict how changes in the preferred curvature affect the force on the stomium and cause the anther to open. We could gain further insight into these conclusions by manipulating the epidermal turgor pressures experimentally. The cell turgor pressure depends upon the difference in osmotic potential across the cell membrane, such that increasing the osmotic potential in the medium surrounding the anther will cause water to flow out of the tissue reducing the epidermal turgor pressures. The model could therefore be used to predict how the anther would open in

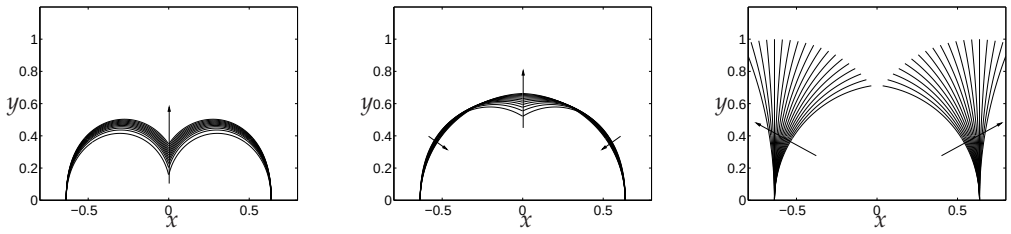

Figure 8: Configurations attained for $\alpha = 1000$, $\beta = 0.01$, $\Phi = 1$, $\lambda_0^- = 1$, $\tilde{\kappa}_0 = 0$, $x_0 = 2/\pi$ and $p = 0$. (a) Solutions for case I (septum intact), with $\lambda_0^+ = 3.5$, and F_{sep} decreasing from 0.0011 to 0 as marked by the arrow. (b) Solutions for case II (septum broken), as dehydration causes λ_0^+ to decrease from 3.5 to 2.5 (at which point the contact force vanishes. (c) Solutions for case III (anther opening), for λ_0^+ decreasing from 2.5 to 0.

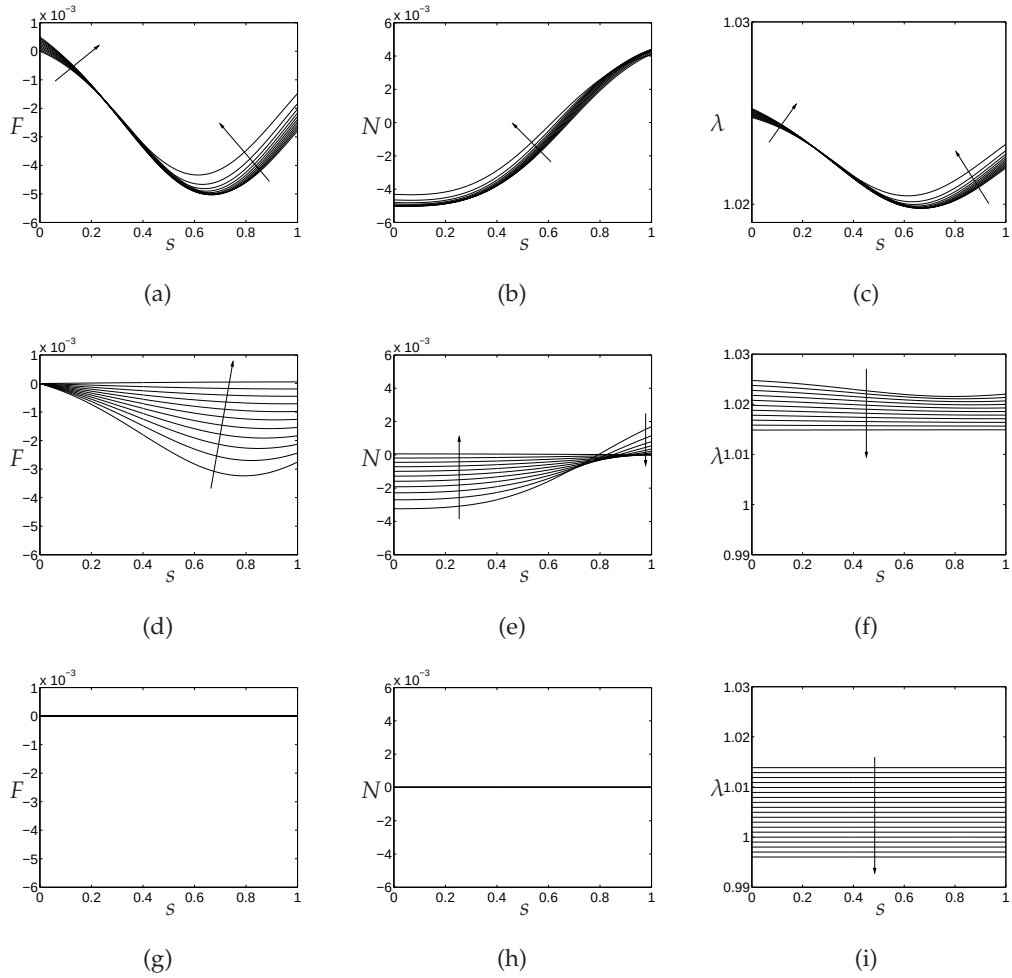

Figure 9: Stresses and strains corresponding to the profiles of figure 8. (a,b,c) Case I – septum intact. (d,e,f) Case II – septum broken. (g,h,i) Case III – anther opening.

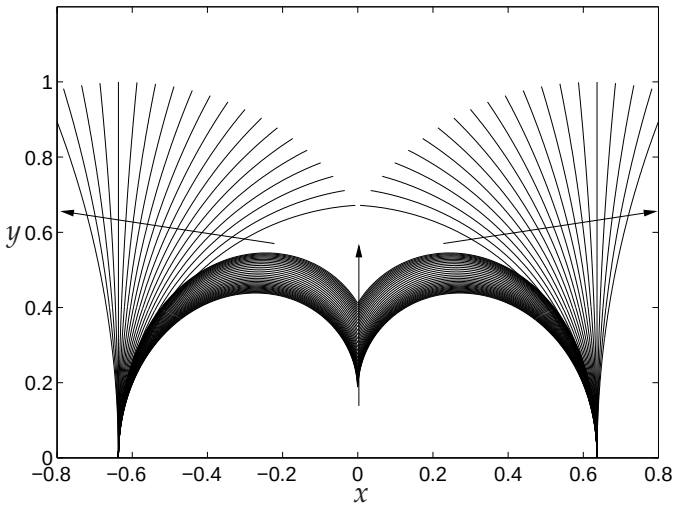

Figure 10: Case II configurations attained for $\alpha = 1000$, $\beta = 0.01$, $\Phi = 1$, $\lambda_0^- = 1$, $\tilde{\kappa}_0 = 0$, $x_0 = 2/\pi$, $p = 0.01$ and λ_0^+ decreasing from 5 to 4.69. For $\lambda_0^+ = 4.69$ the contact force at the stomium vanishes, the anther starts to open and the locule pressure as released ($p = 0$). In the absence of locule pressure the anther may briefly close (not pictured). The anther will open once more as λ_0 is reduced to 2.5 – here we show case III solutions for λ_0 decreasing from 2.5 to 0.5. Arrows indicate decreasing λ_0^+.

response to an increase in the osmotic potential of the medium, and these predictions could be validated experimentally using a similar procedure as described in §1.5 .

The model partially explains the behaviour of the myb26 mutants, for which endothecial secondary thickening does not occur. In our model, this is equivalent to letting $R_f^* \to 0$ so that $D^* \ll 1$. The endothecial bending resistance being small suggests that the configuration of this layer is easily disrupted, potentially resulting in the 'collapsing' of the locule observed experimentally. This behaviour is seen to prevent anther opening. A target for future modelling lies in explaining the behaviour of the myb26 mutant more carefully, with particular regard to the shrinkage of the endothecium observed *in vitro*, which is not explained by our current model.

References

L. Bonner and H. Dickinson. Anther dehiscence in Lycopersicon esculentum Mill. *New Phytologist*, 113:97–115, 1989.

G.A. Costello. Large deflections of helical spring due to bending. *ASCE J. Eng. Mech. Div.*, 103(3):418–487, 1977.

J. Dawson, E. Sözen, I. Vizir, S. Van Waeyenberge, Z.A. Wilson and B.J. Mulligan. Characterization and genetic mapping of a mutation (ms35) which prevents anther dehiscence in Arabidopsis thaliana by affecting secondary wall thickening in the endothecium. *New Phytologist*, 144:213–222, 1999.

C. Keijzer. The processes of anther dehiscence and pollen dispersal. I. The opening mechanism of longitudinally dehiscing anthers. *New Phytologist*, 105:487–489, 1987.

A.E.H. Love. *A treatise on the mathematical theory of elasticity*. Dover publications Inc. New York, USA., 1944.

M.R. Nelson, D. Howard, O.E. Jensen, J.R. King, F.R.A.J. Rose and S.L. Waters. Growth-induced buckling of an epithelial layer. *Biomechanics and Modeling in Mechanobiology*, 2011. doi:10.1007/s10237-010-0280-0.

R.J. Scott, M. Spielman and H.G. Dickinson. Stamen structure and function. *Plant Cell*, 16 Suppl 1:S46–60, 2004.

R. Stadler, E. Truernit, M. Gahrtz and N. Sauer. The AtSUC1 sucrose carrier may represent the osmotic driving force for anther dehiscence and pollen tube growth in Arabidopsis. *Plant J.*, 19:269–278, 1999.

Z.A. Wilson, J. Song, B. Taylor and C. Yang. The final split – the regulation of anther dehiscence. *J. Exp. Botany*, 2011. doi:10.1093/jxb/err014.